1   The influence of calcium, sodium and bicarbonate on the uptake of uranium onto nanoscale

2   zero-valent iron particles

3   *Richard A. Crane,*[1] Huw Pullin[2] and Thomas B. Scott[2]*

4   [1] School of Civil and Environmental Engineering, University of New South Wales,

5   Kensington, NSW 2052, Australia.

6

7   [2] Interface Analysis Centre, School of Physics, University of Bristol, Tyndall Avenue,

8   Bristol. BS8 1TL.

9

10 *Corresponding Author.   E-mail: R.Crane@unsw.edu.au

11

12

13

14

15

16

17

18

19

20

21

22

23

24   **Abstract**

25   This work investigates the influence of calcium (Ca), sodium (Na) and bicarbonate (HCO_3^-)

26   on the uptake of uranium (U) onto nanoscale zero-valent iron particles (nZVI). Batch systems

27   containing U at 1 mg/L and HCO_3^- at 0, 10, 100 and 1000 mg/L were tested with nZVI at 500

28   mg/L. NaCl was also added to the batch systems containing HCO_3^- at 0, 10 and 100 mg/L in

29   order to normalise the ionic strength to the batch system containing HCO_3^- at 1000 mg/L.

30   Comparator systems were tested which contained U at 1 mg/L, HCO_3^- at 0, 10 and 100 mg/L

31   and equal moles of $CaCl_2$ to NaCl in the aforementioned batch systems. Mine water

32   containing a similar concentration of U (1.03 mg/L) was also tested as a natural analogue.

33   Results demonstrate Ca as having no appreciable influence on the capacity of nZVI for U

34   uptake, with >99 % removal recorded for all systems. U desorption was enhanced, however,

35   with 87.3, 85.2 and 84.7 % removal recorded after 672 hours for the 0, 10 and 100 mg/L

36   bicarbonate systems compared with 99.9, 99.7 and 97.1 % recorded for the Na-bearing (Ca

37   absent) systems. Moreover, maximum U removal onto nZVI was directly proportional to

38   HCO_3^- concentration for the Na-bearing systems, whereas no trend was identified for the Ca-

39   bearing systems. Results demonstrate Ca as having a significant inhibitive influence on the

40   long-term retention (e.g. > 48 hours) of U on nZVI, which is independent of HCO_3^-

41   concentration when it is also present at <100 mg/L.

42

43

44

45

46

47   **Keywords:** uranium, nanoscale zero-valent iron particles, bicarbonate, calcium, mine water,

48   remediation

Introduction

A key environmental legacy of mankind's military and civil nuclear activities has been the release of uranium (U) into the environment. U presents a considerable long-term environmental concern and can significantly limit the potential for site redevelopment. In addition, the contamination of groundwater by more soluble forms of U can compromise drinking water sources and spread contamination over significant distances. U mobility in groundwater is governed by its redox, sorption and complexation behaviour. It can exist in many oxidation states [e.g. U(0), U(III), U(IV), U(V) and U(VI)], however, in natural groundwater systems (e.g. $6 < pH < 9$) U(VI) it typically predominates as the uranyl ion (UO_2^{2+}), which is prone to complexation with many ubiquitous groundwater constituents, including: phosphate, silicate, sulphate, fluoride and (bi)carbonate [1]. Consequently, more than 42 dissolved U species, 89 U minerals and 368 inorganic crystal structures that contain U(VI) have been documented [2]. The affinity of U with bicarbonate is of great importance due to the extremely high stability of uranyl carbonate complexes in comparison to the other complexes which form in ground water systems [1]. In the presence of bicarbonate (HCO_3^-) and dissolved calcium (Ca), two ternary aqueous uranyl complexes: $Ca_2UO_2(CO_3)_3$ (log β_{213} = 30.70) and $CaUO_2(CO_3)_3^{2-}$ (log β_{113} = 27.18) become increasingly prominent, and are typically the dominant species in natural groundwater conditions [3]. For example, analysis of groundwater samples taken from a U mill tailing remedial action (UMTRA) site in Tuba City, Arizona, USA, determined that they comprised >99% of the U(VI) in solution [4]. In addition, Fox et al. (2006) [5] recorded a decrease from 77% U(VI) adsorbed on quartz with no dissolved Ca to 10% adsorbed with a Ca concentration of 8.9 mM in carbonate-bearing solution. As a consequence there is a great need for further studies investigating the geochemistry of uranyl-calcium-carbonato complexes, in order to inform the development of new water treatment technologies. In recent years much focus has been applied on the

74   potential utility of nanoscale zero-valent iron particles (nZVI) for the removal of aqueous U

75   from waste waters [6], [7], [8], [9], [10], [11], [12], [13], [14], [15], [16], [17]. Specific

76   mechanistic and kinetic investigations into the removal of uranyl-calcium-carbonato

77   complexes onto nZVI, however, are limited at present [18]. Yan et al., (2010) [17]

78   investigated the uptake of U onto nZVI in anoxic conditions batch systems containing

79   $NaHCO_3$ with and without Ca. The work demonstrated that the kinetics of aqueous U(VI)

80   removal is influenced by both Ca and HCO_3^- concentration, namely that the kinetics of

81   aqueous U(VI) removal in mixed systems (1 mM HCO_3^- and Ca) is comparable to those in

82   systems containing 1mM HCO_3^- or Ca. Overall, the results demonstrate nZVI as highly

83   effective for the removal of U(VI) from anoxic waters for Ca and HCO_3^- concentrations up to

84   1 mM and 10 mM respectively. To the best of our knowledge, however, the long-term (e.g.

85   >96 hours) retention of U on nZVI in the presence of HCO_3^- and/or Ca is yet to be

86   investigated. The objective of this work is to investigate this process in batch systems also

87   containing dissolved oxygen (DO). The work has been established in order to correlate U

88   desorption processes with changes in nZVI corrosion production formation, in order to

89   simulate the eventual recovery of a nZVI subsurface treatment zone to redox conditions prior

90   to nZVI injection. Results are intended to evaluate the long-term integrity of *in situ* U

91   treatment using nZVI, namely the potential for U desorption following the ultimate exposure

92   of the treatment zone to DO.

93

94   **2. Materials and methods**

95   **2.1. Solution synthesis**

96   All chemicals used in this study [$CaCl_2$, C_2H_6O, C_3H_6O, $FeSO_4 \cdot 7H_2O$, HNO_3, NaCl, $NaBH_4$,

97   $NaHCO_3$, NaOH and ($UO_2(CH_3COO)_2 \cdot 2H_2O$)] were of ACS reagent grade and all solutions

98   were prepared using Milli-Q purified water (resistivity >18.2 MΩ cm). Four 400 mL stock

99　　solutions were synthesised comprising U at 1 mg/L and HCO_3^- at 0, 10, 100 and 1000 mg/L

100　　using ($UO_2(CH_3COO)_2\cdot2H_2O$) and $NaHCO_3$ respectively. NaCl was then added at 696, 688

101　　and 625 mg/L to the batch systems containing 0, 10 and 100 mg/L $NaHCO_3$ respectively in

102　　order to equalise their ionic strength with the batch system containing 1000 mg/L $NaHCO_3$.

103　　A further three 400 mL solutions were synthesised comprising U at 1 mg/L, $NaHCO_3$ at 0, 10

104　　and 100 mg/L. Equal moles of Ca to Na that was added to the aforementioned 0, 10 and 100

105　　mg/L $NaHCO_3$ solutions, was also added to the batch systems, which comprised 719, 712 and

106　　647 mg/L of $CaCl_2$ respectively. The pH of all systems was then adjusted to 8.0 using 0.5 M

107　　NaOH. The solutions were stored in sealed glass jars (500 ml Schott Duran) in the open

108　　laboratory prior to analysis and in between sampling intervals.

109

110　　**2.2. U-bearing mine water**

111　　The U-bearing natural water used herein was taken from the Ciudanovita Uranium Mine,

112　　Banat, Romania. The site is valley confined and bounded by limestone ridges which

113　　contribute significant concentrations of dissolved HCO_3^- to ground and surface waters. The

114　　water is used for mining purposes and is pumped from approximately 200 m below sea level.

115　　It initially contains trace concentrations of DO, however, quickly equilibrates with the

116　　atmosphere to reach DO concentrations more typical for that of vadose and/or surface waters

117　　(7–12 mg/L), changing its redox potential and associated U(VI) transport properties in the

118　　process.

119

120　　**2.3. Zero-valent iron nanoparticle synthesis**

121　　Pure nZVI were synthesised following the method first described by Glavee et al., (1995)

122　　[19], and then adapted by Wang and Zhang (1997) [20], which uses sodium borohydride to

123　　reduce ferrous iron to a metallic state. 7.65 g of $FeSO_4\cdot7H_2O$ was dissolved in 50 mL of

124 Milli-Q water (> 18.2 MΩ cm) and then a 4M NaOH solution was used to adjust the pH to

125 6.8. NaOH addition was performed slowly, dropwise, to avoid the formation of

126 hydroxocarbonyl complexes. The salts were reduced to nZVI by the addition of 3.0 g of

127 NaBH$_4$. The nanoparticle product was isolated via centrifugation (Hamilton Bell v6500

128 Vanguard centrifuge, 6500 RPM for 2 minutes), rinsed with Milli-Q water (ratio of 50 mL

129 per g of nZVI) and then centrifuged (Hamilton Bell v6500 Vanguard centrifuge, 6500 RPM

130 for 2 minutes). This step was then repeated but using ethanol and then acetone as the solvent.

131 The nanoparticles were dried in a vacuum dessicator (approx. 10^{-2} mbar) for 48 hours and

132 then stored in an argon filled (BOC, 99.998 %) MBraun glovebox until required.

133

134 **2.4. Experimental procedure**

135 Eight 500 mL Schott Duran jars were each filled with 400 mL of each U-bearing solution. A

136 nZVI mass of 0.2 g (0.5 g/L) was then added. In each case, the nZVI was suspended in 5 mL

137 of ethanol and dispersed by sonication for 30 seconds. Each batch system was sampled at 0 h,

138 0.5h, 1 h, 2 h, 24 h, 48 h, 72 h, 7 d, 14 d and 28 d. Prior to sampling, the jars were gently

139 agitated to ensure homogeneity and pH, Eh and DO measurements were taken using a Hach

140 multimeter (model HQ40d) using a combination gel electrode for pH measurements, a gel-

141 electrolyte reference ORP electrode for Eh measurements, and a luminescent/optical

142 dissolved oxygen (LDO) probe for DO measurements. Aliquots of 5 mL were then taken

143 from each batch system and centrifuged using a Hamilton Bell Vanguard V6500 desktop

144 centrifuge at 6500 rpm for 30 seconds to separate the liquid and solid phases. The supernatant

145 was then decanted, filtered through a 0.22 μm cellulose acetate filter and then prepared for

146 inductively coupled optical emission spectrometry (ICP-OES) and inductively coupled

147 plasma mass spectrometry (ICP-MS) by the additional of 1 % by volume of concentrated

148 HNO$_3$. The solid was prepared for X-day diffraction (XRD) by rinsing with Milli-Q water

149   (ratio of 50 mL per g of nZVI) and then centrifugation (Hamilton Bell v6500 Vanguard

150   centrifuge, 6500 RPM for 2 minutes). This step was then repeated but using ethanol and then

151   acetone as the solvent. The resultant suspension was then pipetted onto a glass optical

152   microscope slide and dried in a vacuum chamber at $<1 \times 10^{-5}$ mbar for 2 hours prior to XRD

153   analysis.

154

155   **2.4. Sample analysis methods**

156   **2.4.1. BET surface area analysis**

157   In preparation for BET surface area analysis, samples were degassed under vacuum (1×10^{-2}

158   mbar) for a 24 hour period at a temperature of 75°C. A known mass of the dried material was

159   then measured using a Quantachrome NOVA 1200 surface area analyser, with N_2 as the

160   adsorbent and following a 7 point BET method.

161

162   **2.4.2. ICP-AES preparation and conditions**

163   Blanks and standards for ICP-AES analysis were prepared in 1 % nitric acid, with Fe

164   standards of 0.10, 0.2, 0.3, 0.4 and 0.5 mg/L. An Agilent 710 ICP-OES (sequential

165   spectrometer) fitted with a cyclone spray chamber and a teflon mist nebulizer was used. The

166   Fe-concentration was measured using the emission line at 234.35 and 259.94 nm.

167

168   **2.4.3. ICP-MS preparation and conditions**

169   Samples for ICP-MS analysis were prepared by performing a 20 times dilution in 1 % nitric

170   acid (analytical quality HNO_3 and Milli-Q water). Blanks and U standards at 1.0, 2.0, 10, 20

171   and 50 μg/L were also prepared in 1 % nitric acid. The ICP-MS instrument used was a

172   Thermo Scientific PlasmaQuad 3.

2.4.4. Transmission electron microscopy

Transmission electron microscopy (TEM) images were obtained with a JEOL JEM 1200 EX Mk 2 TEM, operating at 120 keV. Nanoparticle samples were suspended in absolute ethanol via sonication for 120 seconds and then mounted on 200 mesh holey carbon coated copper grids. The nanoparticle infused grids were then dried in a vacuum chamber at $<1 \times 10^{-5}$ mbar for 2 hours.

2.4.5. X-ray diffraction

A Phillips Xpert Pro diffractometer with a $Cu_{K\alpha}$ radiation source (λ= 1.5406 Å) was used for XRD analysis (generator voltage of 40 keV; tube current of 30 mA). XRD spectra were acquired between 2θ angles of 10–90°, with a step size of 0.02° and a 2 s dwell time.

2.4.6. X-ray photoelectron spectroscopy

A Thermo Fisher Scientific Escascope equipped with a dual anode X-ray source ($Al_{K\alpha}$ 1486.6 eV and $Mg_{K\alpha}$ 1253.6 eV) was used for XPS analysis. Samples were analysed at $<5\times10^{-8}$ mbar with $Al_{K\alpha}$ radiation of 300 W (15 kV, 20 mA) power. High resolution scans were acquired using a 30 eV pass energy and 300 ms dwell times. Following the acquisition of survey spectra over a wide binding energy range, the Fe 2p, C 1s, O 1s and U 4f spectral regions were then scanned at a higher energy resolution such that valence state determinations could be made for each element. Data analysis was carried out using Pisces software (Dayta Systems Ltd.) with binding energy values of the recorded lines referenced to the adventitious hydrocarbon C1s peak at 284.8 eV. In order to determine the relative proportions of Fe^{2+} and Fe^{3+} in the sample analysis volume, curve fitting of the recorded Fe 2p photoelectron peaks

197 was performed following the method of Grosvenor et al. (2004) [21]. The Fe 2p profile was

198 fitted using photoelectron peaks at 706.7, 709.1, 710.6 and 713.4 eV corresponding to Fe^0,

199 $Fe^{2+}_{octahedral}$, $Fe^{3+}_{octahedral}$ and $Fe^{3+}_{tetrahedral}$. These parameters were selected on the basis that the

200 surface oxide was assumed to be a mixture of wüstite and magnetite, as the oxide Fe^{2+} is in

201 the same coordination with the surrounding oxygen atoms in both forms of oxide.

202 **3. Results and discussion**

203 **3.1. Characterisation of the unreacted nanoparticles**

204 Preliminary characterisation of the nZVI was performed using BET surface area analysis,

205 TEM, XRD and XPS. BET surface area analysis determined that the surface area of the nZVI

206 was 16.97 m^2/g. TEM analysis determined that the nZVI were roughly spherical, with an

207 approximate size range of 20-120 nm and an average diameter of 32 nm. The density contrast

208 between the Fe^0 core and oxide shell within the nZVI was not identified and the material was

209 recorded as relatively amorphous. Individual particles were recorded as aggregated into

210 chains and rings, attributed to electrostatic and magnetic attraction forces between adjacent

211 particles. XRD analysis recorded a broad diffraction peak at 44.9º 2θ and two lower intensity

212 peaks at 65.6 and 82.6 2θ, confirming the presence of amorphous Fe^0. XPS analysis recorded

213 the outer surface of the nZVI to be comprised of a mixed valent (Fe^{2+}/Fe^{3+}) oxide. The results

214 are summarised in Table 1.

215

Parameter		nZVI
Particle size distribution (%)	0-50 nm	85
	50-100 nm	8
	>100 nm	7
Crystallinity		Amorphous (α-Fe)

| Surface area (m^2/g)		16.97
Surface composition (%)	Fe	30.5
	O	32.1
	C	14.5
	B	22.9
Surface stoichiometry	$(Fe^0/Fe^{2+} + Fe^{3+})$	0.02
	Fe^{2+}/Fe^{3+}	0.38

216

217 **Table 1.** A summary of the experimental results regarding the bulk and surface properties of

218 the nZVI used in the current work. Note: a significant proportion of the carbon detected is

219 likely to be adventitious carbon.

220
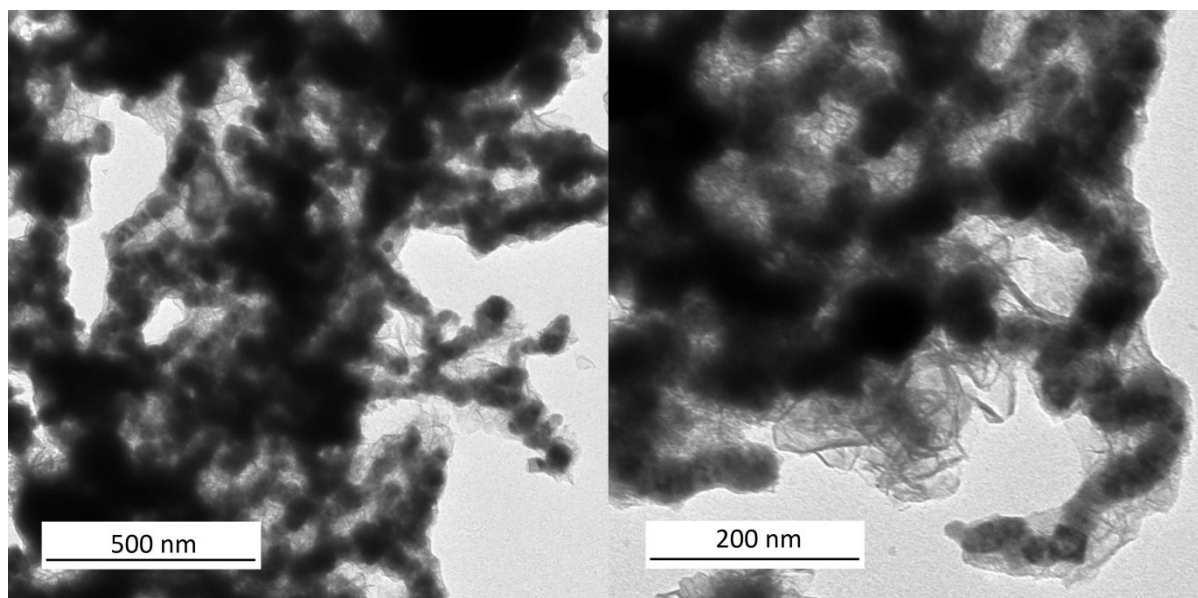
221

222 **Figure 1.** TEM images of the unreacted nZVI.
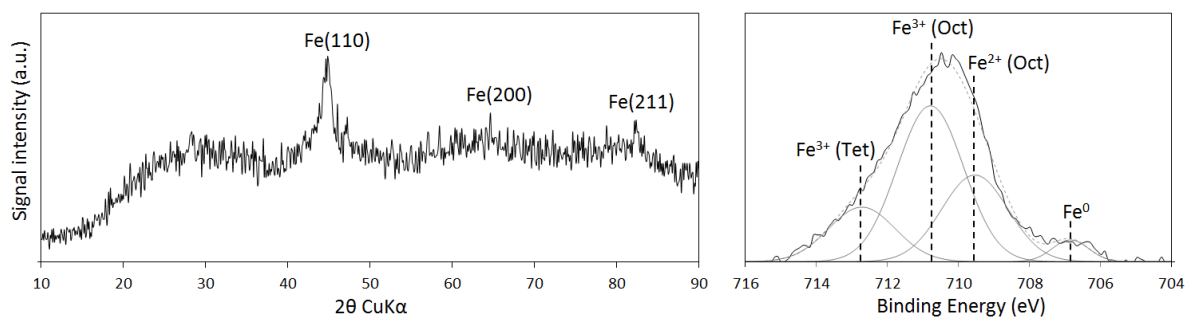
223
224 **Figure 2.** XRD spectra for the range of 10-90° 2θ (LHS) and curve fitted XPS Fe 2p$_{3/2}$

225 photoelectron spectra (RHS) for the unreacted nZVI.

226

3.2. Preliminary characterisation of the U contaminated water

228 Prior to nanoparticle addition, the U-bearing mine water was characterised using ICP-MS

229 (U), ICP-AES (Ca, Mg, Na and U), volumetric titration (HCO_3^-) and ion chromatography

230 (NO_3^- and SO_4^{2-}), with the results displayed in Table 2.

231

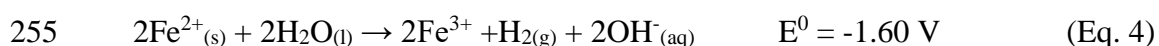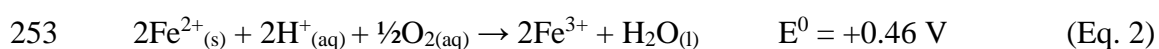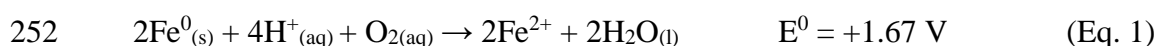| Chemical species	Concentration (mg/L)
Major cations	
Ca	52
Mg	7
Na	652
U	1.03
Major anions	
HCO_3^-	845
NO_3^-	0.9

SO_4^{2-}	65

232

Table 2. Concentrations of U and major ions present in the mine water, analysed by ICP-MS (U), ICP-AES (Ca, Mg, N and U), volumetric titration (HCO_3^-) and ion chromatography (NO_3^- and SO_4^{2-})

3.3. Changes in pH/Eh/DO

Following the addition of the nZVI a rapid shift to strongly chemically reducing conditions was recorded, with Eh less than -350 mV and near-zero DO (<0.5 mg/L) recorded for all batch systems after 30 minutes reaction time (Figure 3). An accompanying increase in pH was also recorded for all systems (Figure 3) with the behaviour therefore attributed to the rapid oxidation of nanoparticulate surfaces, consuming DO and H^+ and increasing the reduction potential of the system (Eq. 1-4). In the early stages of reaction (<30 minutes), the predominant mechanism of nZVI corrosion is considered to have been through reaction with H^+ via the consumption of DO (Eq. 1 and 2). Following this time period the absence of DO dictates that corrosion could only proceed through the direct reaction (hydrolysis) with water (Eq. 3 and 4). Whilst Fe^0 is an essential component of these reactions it is noted that the nZVI used in the current work was determined as having a encapsulating (hydr)oxide layer which was acquired during synthesis (Figures 1 and 2). Fe^0 is therefore considered to only react indirectly with the aqueous solutions and associated dissolved components.

$$2Fe^0_{(s)} + 4H^+_{(aq)} + O_{2(aq)} \rightarrow 2Fe^{2+} + 2H_2O_{(l)} \qquad E^0 = +1.67 \text{ V} \qquad \text{(Eq. 1)}$$

$$2Fe^{2+}_{(s)} + 2H^+_{(aq)} + \tfrac{1}{2}O_{2(aq)} \rightarrow 2Fe^{3+} + H_2O_{(l)} \qquad E^0 = +0.46 \text{ V} \qquad \text{(Eq. 2)}$$

$$Fe^0_{(s)} + 2H_2O_{(l)} \rightarrow Fe^{2+} + H_{2(g)} + 2OH^-_{(aq)} \qquad E^0 = -0.39 \text{ V} \qquad \text{(Eq. 3)}$$

$$2Fe^{2+}_{(s)} + 2H_2O_{(l)} \rightarrow 2Fe^{3+} + H_{2(g)} + 2OH^-_{(aq)} \qquad E^0 = -1.60 \text{ V} \qquad \text{(Eq. 4)}$$

256   For all systems chemically reducing Eh and low DO (<3 mg/L) were maintained for the first

257   24 hours of reaction, with a gradual reversion to ambient conditions recorded onwards from

258   this time. A concurrent decrease in solution pH was also recorded for all systems with the

259   behaviour therefore ascribed to a decrease in the rate of nZVI oxidation (corrosion). No clear

260   trend in Eh, DO or pH change as a function of HCO_3^- concentration can be discerned, with

261   the behaviour recorded to be relatively similar for all systems. This was expected, given that

262   each synthetic solution had an equal ionic strength, which is a key influence on nZVI

263   corrosion rate.

264
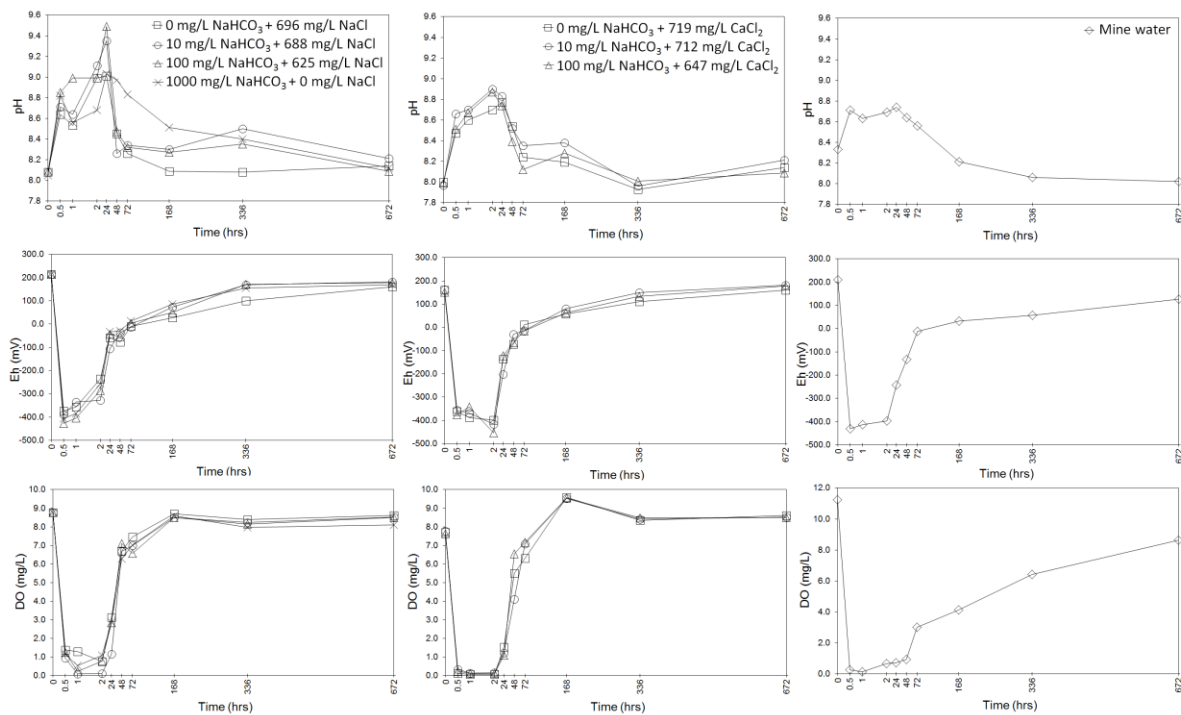
265

266   **Figure 3.** Changes in solution Eh, dissolved oxygen (DO) and pH as a function of reaction

267   time (0-672 hrs) for the batch systems containing nZVI. The control (nanoparticle free) for

268   each batch system (not shown) recorded an Eh variation of <10 mV, a DO variation of <0.2

269   mg/L and a pH variation of <0.05 from the starting solution.

270

271   **3.4. Changes in aqueous U and Fe concentrations**

272 Analysis of liquid samples using ICP-MS recorded rapid $U_{(aq)}$ removal in all systems with

273 removal of >50% recorded after 30 minutes in all systems (Figure 4). It can be noted that

274 relatively similar behaviour was recorded for the batch systems containing 0 and 10 mg/L

275 $NaHCO_3$ (no Ca), with 99.9 % $U_{(aq)}$ removal recorded within the first 24 hours for both

276 systems. Slightly lower U uptake was recorded for the 100 mg/L $NaHCO_3$ (no Ca) batch

277 system, with maximum U removal of 98.8 % U removal recorded after 24 hours. In contrast a

278 maximum of only 62 % U uptake was recorded for the 1000 mg/L $NaHCO_3$ (no Ca) system,

279 with near total re-release occurring from 72 hours onwards. Comparing these results with U

280 uptake data recorded for the batch systems containing Ca it can be noted that for all systems

281 containing Ca similarly high initial U uptake (> 99 %) was recorded in the first 24 hours of

282 reaction, however, desorption of 12.7, 14.8 and 15.3 % was recorded for the batch systems

283 containing 0, 10 and 100 mg/L $NaHCO_3$ (Figure 5). Similar behaviour was also recorded for

284 the U-bearing mine water, with >99.5 % uptake recorded after 30 minutes of reaction, but

285 followed by near-total re-release in the latter stages of the reaction. Overall the results

286 demonstrate that Ca exhibits a strong control on the long-term stability of U on nZVI in

287 waters containing DO and at circumneutral pH.
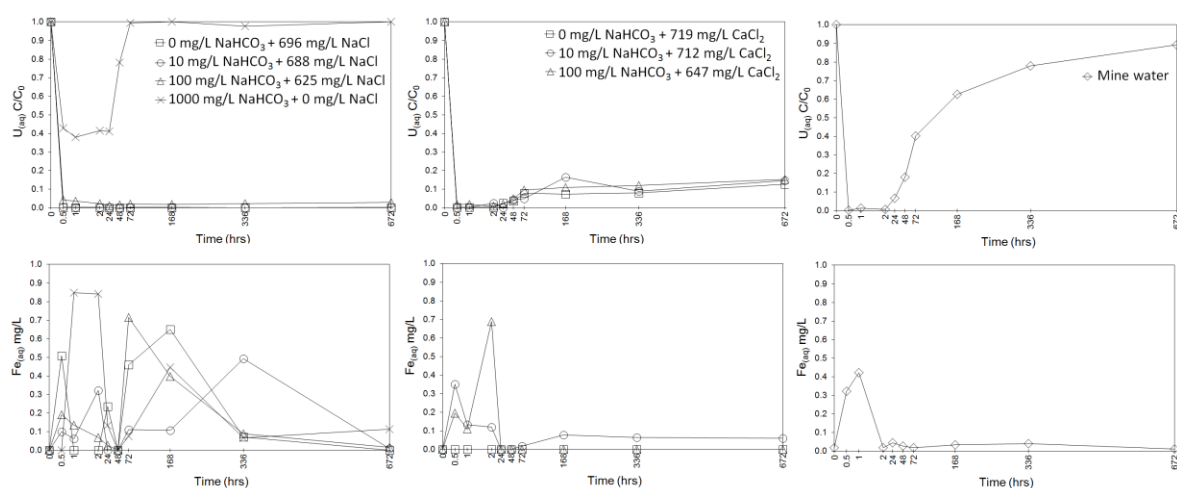
288

289 **Figure 4.** Changes in aqueous U and Fe concentrations as a function of reaction time (0-672

290 hrs) for the batch systems containing nZVI. The control (nanoparticle free) for each batch

291   system (not shown) recorded an aqueous U concentration variation of <0.2 mg/L from the

292   starting solution.

293
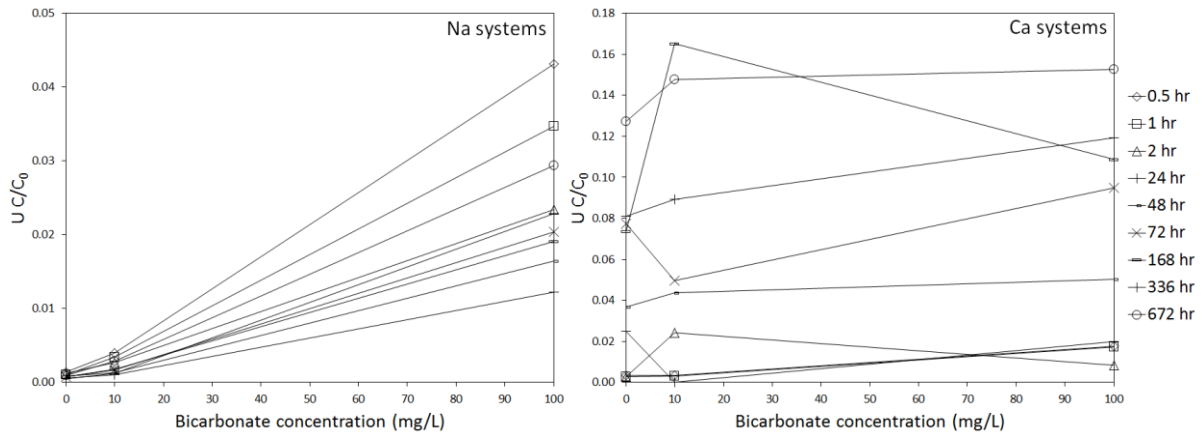
294

295   **Figure 5.** Aqueous U concentration as a function of bicarbonate concentration (0 – 100

296   mg/L) for the batch systems containing Na (LHS) and Ca (RHS).

297

298   **3.5. X-ray diffraction**

299   XRD was used to determine the bulk crystallinity and composition of nZVI solids extracted

300   from all batch systems at periodic intervals during the sorption experiments (Figure 6).

301   During the initial stages of the reaction (≤ 4 hours) a transition from Fe^0, with peaks centred

302   at 44.6 and 82.6° 2θ corresponding to Fe(110) and Fe(211), to a mixture of 2-line ferrihydrite

303   ($5Fe_2O_3 \cdot 9H_2O$) and magnetite (Fe_3O_4) was recorded for all systems. This was not unexpected

304   given that both $5Fe_2O_3 \cdot 9H_2O$ and Fe_3O_4 are common Fe^0 corrosion products in circumneutral

305   and alkaline solutions [22], [23], [24]. In general, $5Fe_2O_3 \cdot 9H_2O$ was the most prevalent

306   corrosion product during the initial stages of nZVI corrosion (e.g. <1 day) with Fe_3O_4

307   emerging as the most prevalent during the latter stages. This was expected, given that Fe_3O_4

308   is known to readily form from $5Fe_2O_3 \cdot 9H_2O$ in near-neutral to basic pH in the presence of

309   HCO_3^-. A mixture of $5Fe_2O_3 \cdot 9H_2O$ and Fe_3O_4 was recorded after 28 days reaction for the

310   mine water and solutions containing $NaHCO_3$ and Na. In contrast, much greater intensity

311   diffraction peaks corresponding to Fe_3O_4 were recorded in the latter stages of the reaction (>

312   1 day) for the batch systems containing $NaHCO_3$ and Ca, indicating that Fe_3O_4 was present in

313   much greater quantity (relative to other corrosion products) and/or crystallinity.

314
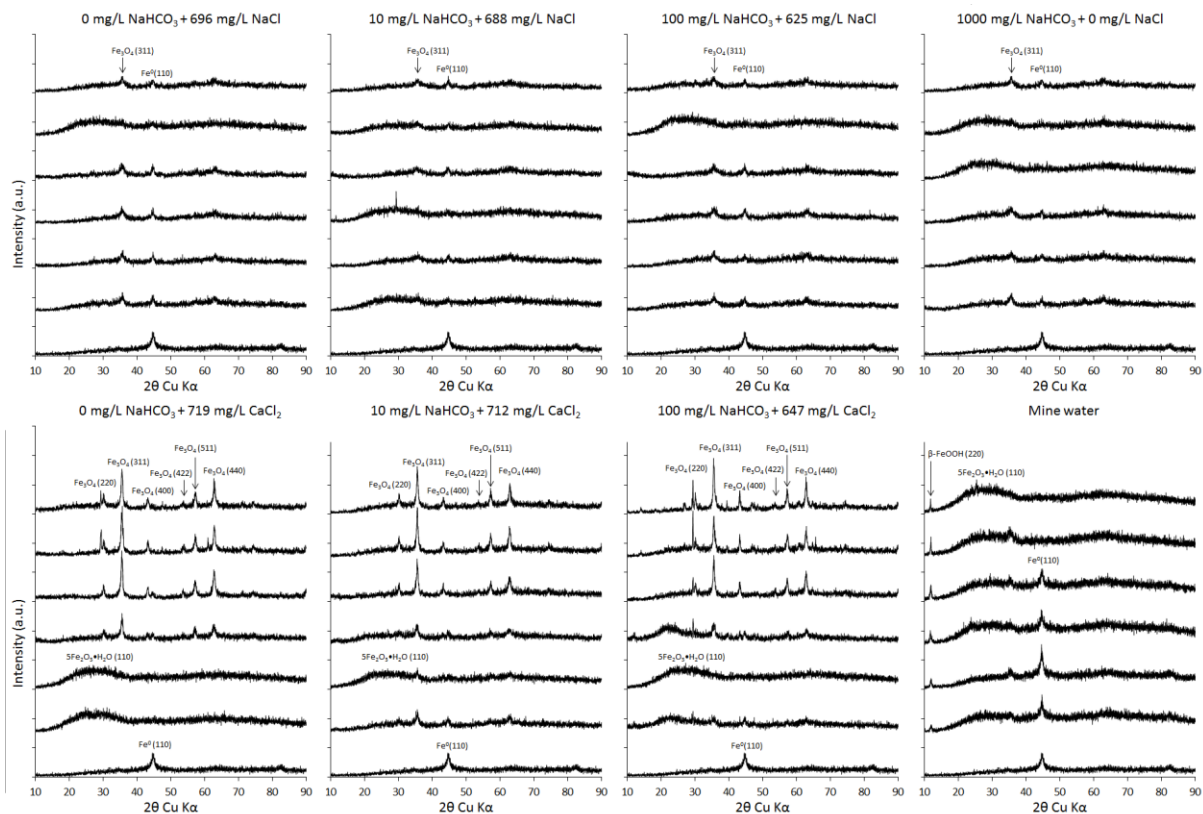
315

316   **Figure 6.** X-ray diffraction spectra for the range of 10-90° 2θ for nZVI extracted from the

317   different solutions after 0h, 1h, 4h, 24h, 48h, 168h and 672h.

318

319   **3.6. Implications for the *in situ* treatment of aqueous U using nZVI**

320   An intrinsic technical challenge associated with the *in situ* treatment of metal and metalloid

321   contaminants (such as U) using nZVI is the prospect for contaminant remobilisation [11],

322   [18]. Ca and HCO_3^- are ubiquitous groundwater constituents, and are also known to

323   significantly enhance the aqueous mobility of U via the formation of uranyl-calcium-

324   carbonato complexes [1]. Indeed it has been demonstrated in recent years that the vast

325   majority of aqueous U present in circumneutral and alkaline pH natural waters is comprised

326 of uranyl-calcium-carbonato complexes, due to their significantly stronger binding affinity

327 compared to other common groundwater constituents [3]. This presents a considerable

328 technical challenge for the treatment of U from natural waters, especially *in situ* treatment

329 applications, where U removal from the aqueous phase must be ensured for long-term (or

330 even quasi-permanent) timescales. The work presented herein has key implications for the *in*

331 *situ* treatment of U using nZVI. It is suggested that because ultimate recovery in DO is a

332 seemingly unavoidable fate for a typical subsurface nZVI treatment zone, associated

333 corrosive transformation of nZVI into (hydr)oxides and a cessation of strongly chemically

334 reducing groundwater conditions (i.e. Eh < -400 mV), is likely to result in considerable U

335 desorption. Indeed considering the significant geochemical perturbation caused by nZVI

336 injection, subsurface treatment zones are often highly metastable, and even a gradual

337 reversion in groundwater conditions toward a pre-injection state may be enough for

338 significant U remobilisation to occur. It is therefore suggested that secondary processes

339 which would maintain strongly chemically reducing conditions (e.g. Eh < -400 mV) within

340 the treatment zone, such as periodic nZVI reinjection and/or capping the treatment zone using

341 an impermeable engineered layer, are essential in order to preserve the long-term

342 performance of nZVI for the *in situ* treatment of U.

343

344 **4. Conclusions**

345 This work presents the influence of Na, Ca and HCO_3^- on the removal of U onto nZVI at pH

346 8. Batch systems containing U at 1 mg/L and HCO_3^- at 0, 10, 100 and 1000 mg/L were tested

347 with nZVI at 500 mg/L. NaCl was also added to the batch systems with HCO_3^- at 0, 10 and

348 100 mg/L in order to normalise the ionic strength. Comparator systems were tested which

349 contained U at 1 mg/L, HCO_3^- at 0, 10 and 100 mg/L and equal moles of $CaCl_2$ to NaCl

350 added to the aforementioned batch systems. Mine water of similar U concentration (1.03

351 mg/L) was also investigated as a natural analogue. Ca had no appreciable impact on the

352 capacity of nZVI for U removal, with >99 % recorded for all systems; however, it

353 significantly enhanced U desorption, with 87.3, 85.2 and 84.7 % removal recorded after 672

354 hours for the 0, 10 and 100 mg/L HCO_3^- systems in comparison to 99.9, 99.7 and 97.1 %

355 recorded for the system with Ca absent. Moreover, in systems were Ca was absent maximum

356 U removal onto nZVI was recorded as directly proportional to HCO_3^- concentration, whereas

357 for systems containing Ca no clear trend was identified. Overall, the results demonstrate Ca

358 as significantly decreasing the long-term stability (e.g. > 48 hours) of U sorbed on nZVI in

359 the presence of DO, with U removal also independent of HCO_3^- concentration when it is also

360 present at <100 mg/L.

361

369

370

371 **References**

[1] K. Ragnarsdottir, L. Charlet, Uranium behaviour in natural environments. Environmental mineralogy – Microbial interactions, anthropogenic influences, contaminated land and waste management. Mineralogical Society Series 9 (2000) 245-289.

[2] S. Regenspurg, D. Schild, T. Schäfer, F. Huber, M.E. Malmström, Removal of uranium(VI) from the aqueous phase by iron(II) minerals in presence of bicarbonate. - App. Geochem. 24 (2009) 1617-1625.

[3] B.D. Stewart, M.A. Mayes, S. Fendorf. Impact of uranyl-calcium-carbonato complexes on uranium(VI) adsorption to synthetic and natural sediments. Env. Sci. Tech. 44 (2010) 928-934.

[4] A. Abdelouas, W. Lutze, E. Nuttall, Chemical reactions of uranium in ground water at a mill tailings site. J. Contam. Hydrol. 34 (1998) 343–361.

[5] P.M. Fox, J.A. Davis, J.M. Zachara, The effect of calcium on aqueous uranium(VI) speciation and adsorption to ferrihydrite and quartz. Geochim. Cosmochim. Acta. 70 (2006) 1379–1387.

[6] R.A. Crane, M. Dickinson, I.C. Popescu, T.B. Scott, Magnetite and zero-valent iron nanoparticles for the remediation of uranium contaminated environmental water. Wat. Res. 45 (2011) 2931-2942.

[7] R.A. Crane, M. Dickinson, T.B. Scott, Nanoscale zero-valent iron particles for the remediation of plutonium and uranium contaminated solutions. Chem. Eng. J. 262 (2015) 319-325.

[8] R.A. Crane, T.B. Scott, The effect of vacuum annealing of magnetite and zero-valent iron nanoparticles on the removal of aqueous uranium. J. Nanotech. 2013 (2013) 1-11 Article ID 173625, 11 pages. doi:10.1155/2013/173625.

[9] R.A. Crane, T.B. Scott, The removal of uranium onto nanoscale zero-valent iron particles in anoxic batch systems. J Nanomater. 2014 (2014) 1-9. doi:10.1155/2014/956360.

[10] R.A. Crane, T.B. Scott, The removal of uranium onto carbon-supported nanoscale zero-valent iron particles. Journal of Nanoparticle Research 16 (2015), 1-13.

[11] R.A. Crane, H. Pullin, J. Macfarlane, M. Silion, I.C. Popescu, M. Andersen, V. Calen, T.B. Scott, Field application of iron and iron-nickel nanoparticles for the ex situ remediation of a uranium bearing mine water effluent. J. Env. Eng. (2015)

[12] M. Dickinson, T.B. Scott, The application of zero-valent iron nanoparticles for the remediation of a uranium-contaminated waste effluent. J. Haz. Mater. 178 (2010) 171-179.

[13] I.C. Popescu, P. Filip, D. Humelnicu, I. Humelnicu, T.B. Scott, R.A. Crane, Removal of uranium (VI) from aqueous systems by nanoscale zero-valent iron particles suspended in carboxy-methyl cellulose. Journal of Nuclear Materials. 443 (2013) 250-255.

[14] O. Riba, T.B. Scott, K.V. Ragnarsdottir, G.C. Allen, Reaction mechanism of uranyl in the presence of zero-valent iron nanoparticles. Geochim Cosmochim Acta. 72 (2008) 4047–4057.

[15] T.B. Scott, I.C. Popescu, R.A. Crane, C. Noubactep, Nano-scale metallic iron for the treatment of solutions containing multiple inorganic contaminants. J. Haz. Mater. 186 (2011) 280-287.

[16] S. Klimkova, M. Cernik, L. Lacinova, J. Filip, D. Jancik, R. Zboril, Zero-valent iron nanoparticles in treatment of acid mine water from in situ uranium leaching. Chemosphere. 82 (2011) 1178-1184.

[17] S. Yan, B. Hua, Z. Bao, J. Yang, C. Liu, B. Deng, Uranium(VI) removal by nanoscale zerovalent iron in anoxic batch systems. Environ. Sci. Tech. 44 (2010) 7783-7789.

[18] R. A. Crane, T.B. Scott, Nanoscale zero-valent iron: future prospects for an emerging water treatment technology. J Haz. Mater. 211 (2012) 112-25.

[19] G.N. Glavee, K.J. Klabunde, C.M. Sorensen, G.C. Hadjipanayis, Chemistry of borohydride Reduction of Iron (II) and Iron (III) Irons in Aqueous and Nonaqueous Media, Formation of Nanoscale Fe, FeB and Fe2B Powders. Inorg. Chem. 34 (1995) 28-35.

[20] C.B. Wang, W.X. Zhang, Synthesizing nanoscale iron particles for rapid and complete dechlorination of TCE and PCBs. Env. Sci. Tech. 31 (1997) 2154-2156.

[21] A.P. Grosvenor, B.A. Kobe, M.C. Biesinger, N.S. McIntyre, Investigation of multiplet splitting of Fe 2p XPS spectra and bonding in iron compounds. Surface and Interface Analysis. 36 (2004) 1564–157.

[22] S. Das, M.J. Hendry, J. Essilfie-Dughan, Transformation of two-line ferrihydrite to goethite and hematite as a function of pH and temperature. Environ. Sci. Technol. 45 (2011) 268-275.

[23] L.E. Davidson, S. Shaw, L.G. Benning, The kinetics and mechanisms of schwertmannite transformation to goethite and hematite under alkaline conditions. Amer. Miner. 93 (2008) 1326-1337.

[24] S. Musi, I. Nowik, M. Risti, Z. Orehovec, S. Popovi, The effect of bicarbonate / carbonate ions on the formation of iron rust. Croatica Chemica Acta. **77** (2004) 141-151.